3rd International Conference on Mechanical Models in Structural Engineering
CMMoST 2015
24-26 June 2015 Seville SPAIN

# Modelling Unreinforced, TRM-strengthened and FRP-strengthened brick masonry walls subjected to eccentric compressive load

**Bernat-Maso, Ernest[1]; Gil, Lluís[2]; Roca, Pere Roca[3]**

## ABSTRACT

The mixed bending/buckling collapse mode of brick masonry walls might be prevented by installing strengthening systems which provide tensile strength. Among others, the Textile Reinforced Mortar (TRM) and Fibre Reinforced Polymers (FRP) laminates are the most common solutions. Their structural response under second order bending effects is studied by means of implementing a numerical simulation adaptable for unreinforced and strengthened walls. The proposed model is based on a bi-dimensional simplification and the use of simplified micromodelling techniques. The use of contact elements has proved to be essential at simulating this type of structures. The obtained results are compared with the experimental evidences on 44 real-scale tests, concluding that the implemented numerical model is accurate at predicting the load-bearing capacity of masonry walls subjected to eccentric compressive loads.

*Keywords: Simplified micromodel; Masonry walls; Fibre Reinforced Polymer; Textile Reinforced Mortar; Cohesive Zone Model.*

## 1. INTRODUCTION

The structural response and failure modes of load-bearing brick masonry walls is characterised by the almost negligible tensile strength of this material. Among the possible collapse mechanisms, the buckling-bending mixed failure is significant because of its sudden development. Using Fibre Reinforced Polymer (FRP) or Textile Reinforced Mortar (TRM) have been proved to be effective strengthening solutions to provide tensile strength and avoid this failure mode in previous researches [1,2].

Strengthening masonry structures with FRP laminates is a common actuation among the conservation and maintenance tasks carried out on masonry buildings which require structural upgrading or rehabilitation. The FRP is specially indicated for those interventions which require limiting the lateral deflection of the walls and look for a less flexible out-of-plane response of the structure because of its outstanding stiffness. However, the drawbacks of this strengthening system (water vapour impermeability and insufficient mechanical compatibility with the masonry), which have been pointed out by several authors (see, for example the work by Baratta et al. [3], or the articles by Papanicolaou

[1] *Department of strength of materials and engineering structures. Polytechnic University of Catalonia (SPAIN). ernest.bernat@upc.edu (Corresponding author)*

[2] *Department of strength of materials and engineering structures. Polytechnic University of Catalonia (SPAIN). lluis.gil@upc.edu*

[3] *Department of Construction Engineering. Polytechnic University of Catalonia (SPAIN). pere.roca.fabregat@upc.edu*

et al. [4,5]), might make other techniques more suitable for general structural interventions on masonry.

This is the case of the TRM (also called Fabric Reinforced Cementitious Matrix, FRCM), which is a composite material consisting of a textile grid embedded into an inorganic matrix. This textile grid should be made of a high strength material like glass, basalt or carbon fibres, whereas the inorganic matrix is typically a cement or lime mortar. It is the physical properties of these inorganic matrixes what allows better physical compatibility with masonry substrates than other adhesives used, for example, in the FRP solutions. In this study field, the experimental studies about the use of TRM at strengthening masonry walls have been focused on analysing the structural response against in-plane loads [6,7] or out-of-plane cyclic loads [8]. However, the second order bending effects on TRM strengthened masonry walls, which might be crucial in non-seismic areas, has deserved less attention, and a few contributions, like [9], are available.

Numerical modelling techniques provide an interesting and inexpensive tool for designing and assessing structures. Nevertheless, little bibliography on the numerical simulation of unreinforced, TRM-strengthened or FRP-strengthened brick masonry walls is available for the case of eccentric compression loading configuration. About the numerical modelling of unreinforced masonry walls, different finite element approaches have been proposed from simplified one-dimensional (1D) beam descriptions approaches (see [10]) to three-dimensional (3D) models, like the one proposed by Martini [11]. Between these two approaches, the sophisticated micro-models presented by Lourenço [12] have to be highlighted. As a compromise between computational cost and result's accuracy, there is a growing tendency to work in homogenised 2D models to represent masonry structures. The required homogenisation techniques have been studied by many researchers ([13,14]).

Regarding the numerical modelling of TRM-strengthened masonry walls, there are only a few publications about the simulation of these type of structures, like the previous work [15]. Similarly, researches dealing with the numerical simulation of the structural response of the TRM as a sole material have been recently published [16], whereas other researchers have studied how to model the TRM-masonry interaction using masonry prisms as reference samples [17]. To some extent, the modelling of TRM reinforced concrete can be considered as a reference case and may provide some insight at modelling TRM reinforced masonry structures. In this line, some authors have dealt with the numerical modelling TRM-strengthened reinforced concrete beams subjected to flexural loading conditions [18], other have been focused on the shear strengthening [19].

Finally, there are not known researches about the numerical simulation of FRP-strengthened masonry walls subjected to eccentric compressive loads which take into account the second order bending effects. However, other structural configurations have been modelled, like the in-plane response [20] or the out-of-plane behaviour [21].

To sum up, there is little research about the numerical modelling of masonry walls subjected to eccentric compressive loads. In addition, there are even less evidences if the considered walls are TRM-strengthened and finally, there are not known studies about the finite element calculation of FRP-strengthened masonry walls subjected to eccentric compressive loads. Thus, the aim of the current

research is to model the mentioned cases and to compare the obtained results to enhance the understanding about the effect of strengthening masonry walls.

## 2. METHODOLOGY

The methodology consisted of implementing a numerical model for predicting the load-bearing capacity of unreinforced brick masonry walls subjected to eccentric compressive loads (see [22]). Then, this model was adapted to take into account the effect of the TRM (see [15]), which is continuously distributed, and the contribution of the FRP, which is applied as discrete laminates following different orientations. It is this last adaptation procedure, the one which is analysed with more detail in this paper. The three resulting numerical models are to be understood as the same approach that evolved so it is significant to describe, compare and discuss the adaptability of the model to the different structural configurations. Comparison with experimental results is also provided to assess the accuracy of the model.

### 2.1. Samples

Forty-four full scale brick masonry walls were tested up to failure due to an eccentrically applied compressive load. All walls were tested in a pinned-pinned configuration with the aim of clearly identifying the boundary conditions and to ease the comparison with the numerical models. Twenty of these walls were unreinforced (W#1-W#20), nine were TRM-strengthened (W#21-W#29) and fifteen were FRP-strengthened (W#30-W#44). In the corresponding cases, the strengthening system (TRM or FRP) was placed on the side of the wall subjected to tensile stresses. The main geometric characteristics of these structures and the corresponding typology of strengthening are summarised in Tables 1, 2 and 3. The first five columns of these tables correspond to the name of the wall, the width of the wall, b, the effective height of the wall, $H_{ef}$ (measured in vertical direction between the two hinges used to set the pinned-pinned configuration), the thickness of the wall, t, and the eccentricity of the load at mid-height at the beginning of the test, $e_0$. The last column presents the dimensionless measurement of the load-bearing capacity of the wall, $\phi$, calculated as the experimental maximum applied force out of the maximum compressive force that a cross section of the wall could bear under uniform stress distribution hypothesis. For the unreinforced cases (Table 1), the compressive strength of the masonry, $f_c$, and its flexural strength, $f_x$, are presented in the sixth and seventh columns respectively. The Young's modulus of the masonry was 780MPa for unreinforced and TRM-strengthened walls and the average density of the used masonry was 1732kg/m$^3$ for all cases. For the TRM-strengthened cases the compressive strength of the masonry was 10.8MPa, its flexural strength was 0.36MPa (see [2]). The last five columns in Table 2 are dedicated to characterise the TRM and they include the type of strengthening mortar (M for the Portland based mortar, R for the lime-based mortar and X for the pozzolanic mortar as presented in [2]), the type of fibre grid (G for glass and C for carbon), the presence of connectors, the number of fibre grids installed into the mortar layer and the real thickness of the TRM layer.

Finally, the strengthening patterns of the FRP-strengthened walls are detailed in Table 3. Columns sixth to ninth present the number of vertical laminates uniformly distributed on the width of the strengthened face, $\#_{v,FRP}$, the number of horizontal laminates uniformly distributed on the height of the strengthened face, $\#_{h,FRP}$, and the number of inclined laminates placed at the same section – constant height –, $\#_{i,FRP}$, considering two directions at an angle of $\pm\alpha$ (°).

**Table 1.** Geometry of the unreinforced brick masonry walls

| Wall | b (mm) | $H_{ef}$ (mm) | t (mm) | $e_0$ (mm) | $f_c$ (MPa) | $f_x$ (MPa) | Φ(%) |
|---|---|---|---|---|---|---|---|
| W#1 | 900 | 2,947 | 132 | 5.6 | 18.2 | 0.23 | 7.8 |
| W#2 | 900 | 2,927 | 132 | 19.6 | 12.9 | 0.36 | 4.3 |
| W#3 | 870 | 2,922 | 132 | 1.2 | | | 8.7 |
| W#4 | 870 | 1,980 | 132 | 7.0 | | | 37.8 |
| W#5 | 900 | 2,917 | 132 | 33.7 | | | 15.6 |
| W#6 | 875 | 2,857 | 132 | 13.1 | 13.7 | | 1.8 |
| W#7 | 885 | 2,872 | 132 | -7.6 | | | 8.3 |
| W#8 | 879 | 2,942 | 132 | 21.5 | | | 8.0 |
| W#9 | 888 | 2,892 | 132 | 0.2 | | | 6.7 |
| W#10 | 888 | 1,865 | 132 | 13.9 | 10.8 | | 33.0 |
| W#11 | 870 | 1,892 | 132 | 1.6 | | | 28.9 |
| W#12 | 882 | 1,841 | 132 | 31.8 | | | 36.7 |
| W#13 | 900 | 1,861 | 132 | 21.2 | | | 6.5 |
| W#14 | 900 | 1,861 | 132 | 29.0 | | | 40.4 |
| W#15 | 895 | 1,845 | 132 | 19.5 | | | 18.4 |
| W#16 | 894 | 1,860 | 132 | 88.0 | | | 31.8 |
| W#17 | 894 | 1,905 | 270 | 20.8 | | | 38.3 |
| W#18 | 871 | 1,197 | 132 | 30.3 | | | 62.6 |
| W#19 | 871 | 1,220 | 132 | 33.0 | | | 53.5 |
| W#20 | 868 | 1,865 | 132 | 5.6 | | | 11.9 |

**Table 2.** Geometry of the TRM-strengthened brick masonry walls

| Wall | b (mm) | $H_{ef}$ (mm) | t (mm) | $e_0$ (mm) | TRM mortar | Fibre grid | Connectors | # fibre grids | $t_{TRM}$ (mm) | Φ(%) |
|---|---|---|---|---|---|---|---|---|---|---|
| W#21 | 865 | 1,832 | 132 | 30.3 | M | G | 0 | 1 | 13.0 | 24.3 |
| W#22 | 872 | 1,827 | 132 | 33.2 | M | G | 0 | 1 | 8.0 | 26.4 |
| W#23 | 868 | 1,822 | 132 | 33.9 | R | G | 0 | 1 | 9.5 | 21.9 |
| W#24 | 867 | 1,840 | 132 | 25.4 | R | G | 0 | 1 | 9.0 | 23.1 |
| W#25 | 868 | 1,828 | 132 | 32.7 | R | G | 0 | 2 | 7.5 | 33.5 |
| W#26 | 869 | 1,823 | 132 | 29.7 | M | G | 0 | 2 | 8.0 | 31.5 |
| W#27 | 873 | 1,822 | 132 | 30.4 | X | C | 0 | 1 | 8.0 | 27.8 |
| W#28 | 871 | 1,828 | 132 | 23.7 | X | C | 6 | 1 | 9.0 | 25.2 |
| W#29 | 868 | 1,827 | 132 | 31.4 | X | C | 9 | 1 | 11.0 | 26.7 |

Three failure modes were experimentally observed: the mixed bending/buckling failure of most of the unreinforced brick masonry walls due to the mechanism formation collapse (a masonry joint opened), the tensile failure of the TRM associated with a mechanism formation process (only for W#21 and W#23) and the shear/compressive failure near the endings of the wall for the rest of the strengthened walls. The real geometric imperfections were measured and introduced into the numerical model through the geometry definition later on. The measurement process consisted on determining the distance between a vertically aligned profile and the wall when it was placed in the testing position. A laser sensor was used for this purpose and measurements were carried out every two masonry rows at the two largest edges of one of the two biggest faces of the walls. These measurements allowed determining the shape of the wall.

**Table 3.** Geometry of the FRP-strengthened brick masonry walls

| Wall | b (mm) | $H_{ef}$ (mm) | t (mm) | $e_0$ (mm) | $\#_{v,FRP}$ | $\#_{h,FRP}$ | $\#_{i,FRP}$ | α (˚) | Φ(%) |
|---|---|---|---|---|---|---|---|---|---|
| W#30 | 837 | 1,798 | 126.5 | 29.5 | 2 | 0 | 0 | --- | 27.3 |
| W#31 | 840 | 1,815 | 125.9 | 31.9 | | | | | 28.6 |
| W#32 | 838 | 1,798 | 126.1 | 29.8 | | | | | 28.9 |
| W#33 | 829 | 1,811 | 126.4 | 29.7 | 3 | 0 | 0 | --- | 31.5 |
| W#34 | 833 | 1,814 | 126.3 | 31.2 | | | | | 31.5 |
| W#35 | 837 | 1,824 | 126.3 | 29.4 | | | | | 39.2 |
| W#36 | 843 | 1,788 | 126.1 | 29.4 | 2 | 2 | 0 | --- | 31.3 |
| W#37 | 835 | 1,792 | 124.4 | 32.7 | | | | | 31.9 |
| W#38 | 827 | 1,797 | 124.7 | 30.1 | | | | | 33.1 |
| W#39 | 833 | 1,777 | 123.8 | 28.7 | 3 | 5 | 0 | --- | 29.1 |
| W#40 | 830 | 1,784 | 124.7 | 27.2 | | | | | 27.9 |
| W#41 | 831 | 1,761 | 124.5 | 27.6 | | | | | 24.1 |
| W#42 | 826 | 1,830 | 124.3 | 26.8 | 0 | 0 | 4 | 61 | 34.5 |
| W#43 | 831 | 1,831 | 124.6 | 28.8 | | | | | 24.0 |
| W#44 | 827 | 1,812 | 123.8 | 27.4 | | | | | 30.7 |

## 2.2. Numerical model for unreinforced cases

The implemented models assume the hypothesis of plane strain applied to simplify the three-dimensional (3D) real case into a bi-dimensional (2D) model. In addition, simplified micromodelling has been used because this approach does not require so much information of the material properties as detailed micromodelling but performs better than macromodels. The proposed method models each brick together with the surrounding mortar as a homogenised material, called masonry, and uses the corresponding experimental properties. Finally, the numerical model considers large deformations to accurately represent the buckling phenomena originated by the second order bending effects. The definition of materials, contacts and geometry have been set as general as possible to assure that the model can be reproduced in general purpose Finite Element Analysis (FEA) packages, like the used one: ANSYS®.

### *2.2.1. Geometry*

The geometric model is defined as a series of piled rectangular parts corresponding to the different masonry rows existing in the analysed wall. Two extra bodies, which are two triangles, one at each end of the wall (see Figure 1), are defined to easily represent the hinges of the pinned-pinned configuration considered for all cases. These triangles allow placing the load application point accurately and setting the rotation axes. In addition, the real shape of each wall is used to create the corresponding model, taking into account its initial out-of-plane imperfections, which might affect the development of second order bending effects.

### *2.2.2. Materials and contacts*

The mechanical response of the brick masonry is orthotropic because of the pattern of the joints. In addition, depending on the properties of the components (units, mortar and interfaces) of this composite material, the masonry shows different failure modes. This complex response is not considered to avoid using advanced simulation tools, which would be against the first aim of the implemented models: keeping them as simple as possible.

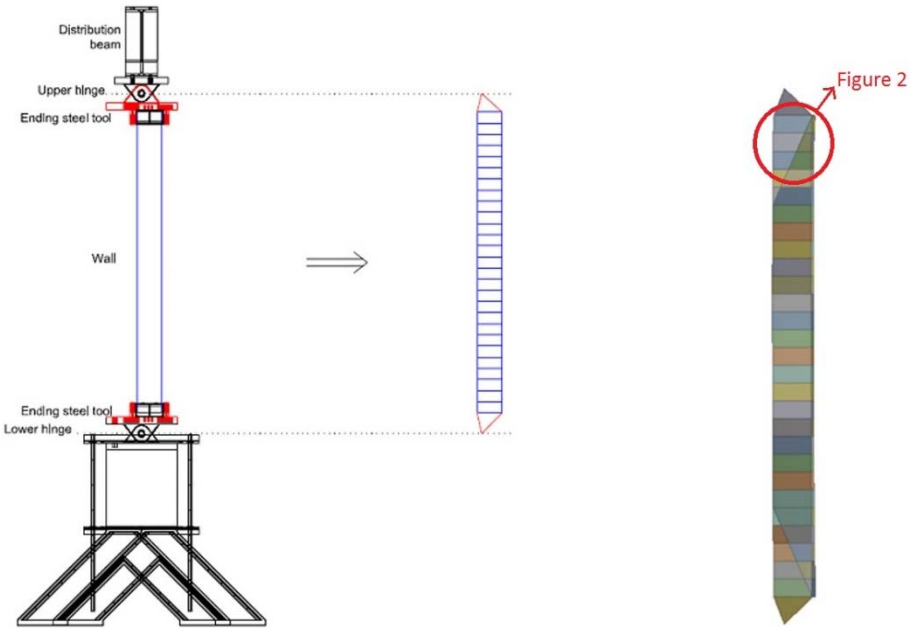


**Figure 1.** *Geometric definition of a general wall*

Thus, masonry is modelled as a homogeneous material, whose compressive response is defined with an isotropic linear elastic with perfect plasticity constitutive model. Thus, only the compressive strength and the Young's modulus are required to characterise the compressive response in the model. On the other hand, the tensional behaviour is controlled by contact elements, which have neither thickness nor elastic properties. The current steel definition included in the FEA software is used to model the material of the parts corresponding with the hinges.

Apart from the experimentally determined properties of the masonry presented before (see section 2.1), the Poisson's coefficient is set to 0.35. This assumption is based on bibliographic evidences like the work by Bosiljkov et al. [23], who proposed values of Poisson's ratio up to 0.4 when using mortar with low content of cement. In fact, according to these authors, the highest Poisson's values corresponded with the lowest values of Young's modulus.

The tensile response of the masonry is modelled using contacts, which are placed between masonry rows. These contacts are "bonded" at the first calculation step, meaning that the corresponding nodes of the adjacent parts are set to move equally and together. The stress increase on every contact, which is associated to the step by step loading process described in section 2.2.4, might cause the opening (debonding) of these contacts accordingly with a bilinear constitutive law. This response is implemented using a cohesive zone model (CZM) that was originally proposed by Alfano et al. [24]. The CZM sets an elastic behaviour up to the brittle failure of the contact. When the tensile strength is reached, the contact opens and the corresponding stress decreases linearly with a slope that is defined by the corresponding fracture energy. Thus, only two parameters (tensile strength and the corresponding

fracture energy) are required to use CZM and it is believed that this is the simplest and most general way to represent the tensile response of the masonry.

The flexural tensile strength, $f_x$ (summarised in Table 1), which was experimentally determined carrying out bond-wrench tests, is used instead of the direct tensile strength in the CZM definition. It is because the flexural tensile strength is considered to be more representative of the response of the masonry under the second order bending phenomena. In fact, the contacts between masonry rows can be bended or compressed but not subjected to a tensile axial effort under the considered loading configuration. In addition, the fracture energy, $G_f^I$, is estimated using Eq. (1). This expression has been adjusted using the experimental results presented in [25] and was previously used in [26,27].

$$(N/m)\ G_f^I = 36.65 \cdot f_x\ (MPa) \tag{1}$$

The sliding failure between masonry rows is not considered because it was not experimentally observed. Finally, as long as the tested walls and the steel hinges were always in contact during the experiments, the debonding process is not considered in these contacts.

### *2.2.3. Mesh*

Figure 2 shows a typical mesh. Masonry is meshed with 8-nodes uniform structured quadrilateral elements with quadratic integration of the displacements. The average size of the elements is 5mm for the masonry of the walls with an effective height below 2m, and 20mm for the taller walls. The parts representing the steel hinges (triangles) are meshed with an unstructured uniform mesh composed by 6-nodes triangular elements and 8-nodes quadrilateral elements with quadratic integration of the displacements and an average size of 5mm.

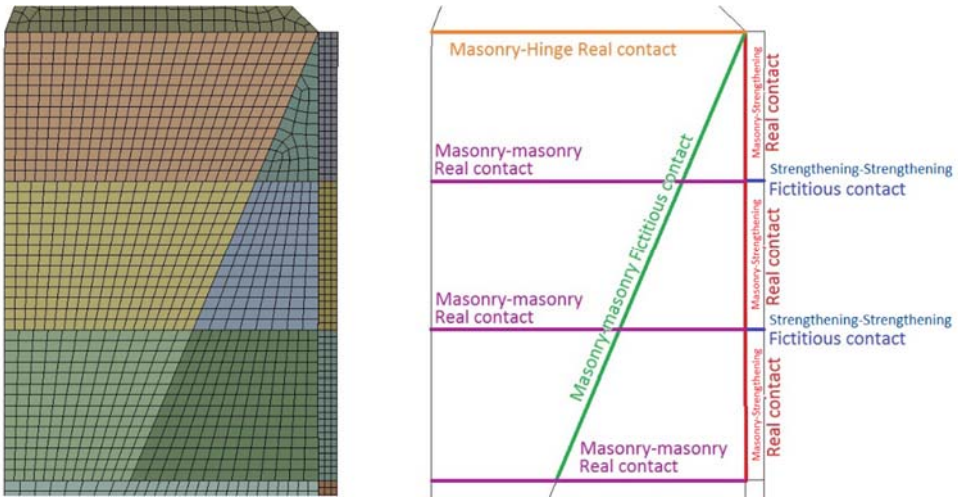


**Figure 2.** *Finite Element mesh and position of the contacts for strengthened walls*

### *2.2.4. Boundary conditions and loading process*

The boundary conditions of the model consisted of fixing the displacement of the lower hinge by restraining the horizontal and vertical movements of the lowest vertex of the corresponding triangular. Additionally, the horizontal displacement of the top vertex of the triangular part representing the upper

hinge is fixed. These constrains allow the structure to rotate around the restrained nodes while impeding any possible lateral displacement at the wall's ends.

The load is indirectly applied as a vertical descending displacement of the top vertex of the model. This movement is applied at a constant rate (step by step calculation) and the force reaction at the application point is taken as the measurement of the applied load for comparing with the experimental values. This displacement-controlled simulated loading process makes it possible to calculate some steps after reaching the maximum load, clarifying the interpretation of the failure pattern. The calculation is performed step by step so each new displacement increase is applied on the deformed configuration of the wall due to the previous loading steps.

### 2.3. Adaptation of the numerical model for the TRM-strengthened cases

The previously described numerical model for unreinforced brick masonry walls was updated to include the possibility of calculating TRM-strengthened walls subjected to eccentric compressive loads. This adaptation required modifying the geometry, the materials and contact descriptions and the mesh definition. Only the modifications are described below so the rest of the definition is the same than for unreinforced masonry walls.

#### *2.3.1. Geometry*

Two main changes in the geometry were necessary to represent the TRM-strengthened walls: a) considering additional parts to model the TRM layer and b) dividing the masonry parts near the ends of the walls following an inclined line to allow the compressive/shear failure of the masonry observed in the experimental tests.

The TRM layer was modelled using rectangular bodies placed next to the ones representing the masonry. There were as many TRM parts as masonry rows and the contacts between them were defined to allow the tensile failure of the TRM, which was observed in two experimental cases (see [2]). The interfaces between masonry parts and TRM parts were also described by means of contact elements. The thickness of the TRM parts was considered constant along the wall's height and equal to real TRM thickness at mid-height for every wall.

In addition, fictitious contacts were placed in an inclined line crossing and dividing the masonry bodies near the extremes of the walls (see Figure 1) to model the compressive/out-of-plane shear collapse mode, which was experimentally observed in most of the TRM strengthened walls. This failure mode was characterised by the opening of one diagonal crack, which always started from one extreme of the strengthened side of the wall and grew to the compressed side of the structure. The chosen orientation for these dividing lines was set to be constant and corresponded to the average inclination of the experimental collapses.

#### *2.3.2. Materials and contacts*

The compressive behaviour of the TRM is governed by the mortar matrix, whereas the tensile response is influenced by a) the mortar matrix (at low loads, before cracking and mobilising the fibre mesh), b)

the fibre grid and c) the adherence between the mortar matrix and the fibre grid (at larger loads, after cracking). Thus, it is a complex response which depends on different parameters. However, a simplified material model was used to represent the TRM to assure an efficient calculation of the load bearing capacity of the TRM strengthened walls. Hence, TRM was modelled as an isotropic and homogeneous material in compression. Its compressive response was set to be linear elastic with perfect plasticity, whereas the tensile response was controlled by the contact elements defined using the CZM.

The compressive behaviour of the TRM is defined by the Young's modulus ($E_m$) and compressive strength the strengthening mortar ($f_{cm}$), whose values are summarised in Table 4. The first variable was experimentally determined whereas the Young's modulus was provided by the producer of the mortar.

**Table 4.** Properties of the strengthening mortars for the TRM solutions

| Mortar | Flexural strength, $f_{xm}$ (MPa) | Compressive strength, $f_{cm}$ (MPa) | Bonding strength, $f_{bm}$ (MPa) | Modulus of elasticity, $E_m$ (MPa) |
|---|---|---|---|---|
| M | 8.1 (0.18) | 42.2 (0.27) | 2 * | 11000 * |
| R | 6.6 (0.03) | 14.5 (0.08) | 0.8 * | 8000 * |
| X | 9.4 (0.10) | 34.5 (0.08) | 0.8 * | 15000 * |

Depending on the location of the contacts (see Figure 2), these might be classified into real contacts and fictitious contacts. The first ones corresponded with the joints of the masonry (described in section 2.2.2) and the interface between the TRM and the masonry. In contrast, the second ones were set in order to allow the development of the experimentally observed failure modes. All contacts for TRM-strengthened walls are summarised in Table 5.

**Table 5.** Properties of the contacts for the TRM walls

| Contact | Walls | Contact Failure | $f_{xt}$ (MPa) | $G_f^I$ (N/m) | $\tau_{max}$ (MPa) | $G_f^{II}$ (N/m) |
|---|---|---|---|---|---|---|
| Real. Masonry-TRM | All TRM | None | --- | --- | --- | --- |
| Fictitious. Masonry-Masonry (inclined) | All TRM | Debonding and Sliding | 2.8* | 100 | 0.56 | 20 |
| Fictitious. TRM-TRM | W#21 W#22 | Debonding | 8.1 | 295 | --- | --- |
| | W#23 W#24 | Debonding | 6.6 | 240 | | |
| | W#25 | Debonding | 12.0 | 440 | | |
| | W#26 | Debonding | 11.3 | 412 | | |
| | W#27 | Debonding | 20.0 | 733 | | |
| | W#28 | Debonding | 17.8 | 652 | | |
| | W#29 | Debonding | 14.5 | 533 | | |

* This value corresponds to the direct tensile strength, not to the flexural tensile strength.

The real contacts between masonry and TRM parts were defined as "bonded", so neither opening nor sliding processes are allowed, which corresponded to the experimental observations. The fictitious contacts between pairs of TRM parts were defined to allow the opening but not the sliding between TRM parts. Thus, they make the TRM tensile failure (experimentally observed in walls W#21 and W#23) possible. This tensile response follows a bilinear constitutive law, which is characterised by the tensile strength and the corresponding fracture energy. The first parameter, $f_{xt}$, is calculated as the maximum

between: (a) the flexural tensile strength of the strengthening mortar and (b) the direct tensile strength of the fibre grid uniformly distributed on the area of the TRM section. In the case (a) the tensile force associated with the flexural tensile stresses on the mortar of the TRM is greater than the direct tensile resistance of the fibre grid embedded, which actually works in direct tension. On the other hand, the case (b) assumes that the force associated with tensile strength of the fibre grid (45kN/m for the used glass fibre grid and 160kN/m for the used carbon fibre grid) is greater than the resistance developed by the mortar in bending configuration. Thus, in the case (b) the fibre grid can bear larger load in direct tension than the mortar matrix up to its bending cracking time. It has to be noticed that (b) is the most likely case for practical strengthening applications. For these contacts the corresponding fracture energy was calculated using the expression presented in Eq. (1).

The second type of fictitious contacts were used in the two inclined lines that divide the five masonry rows near each end of a single wall to simulate the compressive/shear failure observed in most of the experimental tests on TRM strengthened walls (and for all of the FRP-strengthened walls later on). These enabled the debonding and the sliding possibilities. Both tensile and shear responses were characterised by bilinear constitutive laws defined by the tensile or tangential strength and the corresponding fracture energy (first, $G_f^I$, and second, $G_f^{II}$, modes respectively). The tensile strength between two masonry parts of the same row, which were separated by the inclined discontinuity, was taken to be equal to the direct tensile strength of the ceramic pieces because the direct tensile strength is understood to be more representative than the flexural one. The corresponding fracture energy was also calculated using Eq. (1).

The shear strength ($\tau_{max}$) was analytically calculated from the experimental data as showed below in Eq. (2). The corresponding fracture energy is calculated using Eq. (1) where the flexural strength is replaced by the shear strength.

$$\tau_{max} = \frac{T}{bm} \tag{2}$$

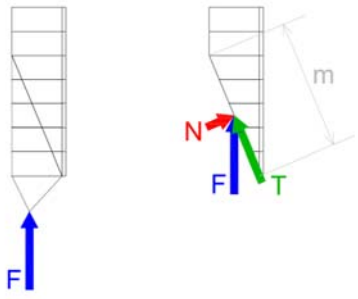


**Figure 3.** *Normal and tangential force components on the failure plane*

The load components, which are normal (N) and tangential (T) to the failure plane, are calculated from the maximum applied force (F) and the observed failure modes (inclination of the crack in walls W#22 and W#24 to W#29) as shown in Figure 3. Then, the tangential component (T) is supposed to be

uniformly distributed on the area (b·m) of the observed discontinuity plane. This allows obtaining the maximum shear strength, where b is the width of the wall and m the length of the failure plane.

It has to be highlighted that the used CZM model considers both fracture processes (opening and sliding of the contact) together, so the shear response is sensible to the normal response and vice versa. The mixed failure criterion characterised by the power law energy criterion presented in the following Eq. (3) is used, where $G^{I}$ and $G^{II}$ are, respectively, the normal and tangential energy of fracture for the case of combined failure.

$$\frac{G^{I}}{G_f^{I}} + \frac{G^{II}}{G_f^{II}} = 1 \tag{3}$$

*2.3.3. Mesh*

8-nodes uniform structured quadrilateral elements with quadratic integration of the displacements with an average size of 3mm was used to mesh the TRM.

**2.4. Novel adaptation of the numerical model for the FRP-strengthened cases**

The previously described numerical model for TRM-strengthened brick masonry walls has been adapted to consider the use of discrete FRP laminates instead of continuous TRM layers. The required modifications are described below so the rest of the definition is the same than for TRM-strengthened walls.

*2.4.1. Geometry*

Similarly to the TRM, the FRP has been modelled as a group of rectangles (1.2mm thickness) in the bidimensional section for all the analysed strengthening patterns. These rectangles correspond to the division of the strengthening layer in as many parts as masonry rows are defined. These divisions allows implementing different definitions of the masonry-FRP contacts to model the restraining effect of the crossed strengthening patterns (W#36-44).

*2.4.2. Materials and contacts*

In contrast to the previous simulations, the design compressive strength of the masonry has been calculated on the basis of the work by Brencich et al. [28], to improve the previous models. These authors suggested that the eccentric compressive strength (21.3 MPa) might be calculated from the concentric compressive strength (18.1 MPa) using the analytical expression presented in equation 15 of [28]. In addition, the representative relationship between the Young's modulus and the compressive strength, which is defined in the fourth table of the work by Brencich et al. [28], is used too. A ratio of $E/f_c = 120$ is assumed taking into account the data presented in this reference and a Young's modulus of 2560 MPa is obtained applying this ratio. The flexural strength, density and Poisson's coefficient of the masonry had the same value than for the previous models.

FRP is also defined as isotropic linear elastic in compression, although this assumption is not significant since the FRP is only considered to be placed on the side of the wall where tensile efforts were developed. The contacts associated with the models of the FRP-strengthened walls that change from the previous ones are: the real contact between masonry and FRP and the fictitious contacts between

FRP parts. The first ones have been defined to allow the sliding (defined by the shear strength, $f_{sFRP}$, and the corresponding fracture energy $G_{f\,int}^{II}$) and debonding (defined by the bonding strength, $f_{bFRP}$, and the corresponding fracture energy $G_{f\,int}^{I}$) phenomena. The FRP-FRP contacts have been set to be "bonded" because no tensile failure of the FRP was observed in the experimental tests.

Moreover, considering the bidimensional simplification of the FRP strengthening system requires a non-conventional material definition. In this line, the density ($\rho_{FRP}$), Young's modulus ($E_{FRP}$), FRP-masonry bonding strength ($f_{bFRP}$), FRP-masonry tangential strength ($f_{sFRP}$) and tensile strength of the FRP ($f_{tFRP}$) are modified to represent the real amount of FRP laminate distributed along the width of the wall. Only the vertical laminates (or part of the vertical component of the inclined ones) are considered in this simplification accordingly with the experimental results. The modified variables have been calculated from the original ones using equation Eq. (4) or Eq. (5) depending if the laminates were vertical or inclined respectively. In this last case, only ¾ parts of the capacity of the installed laminates is considered in agreement with the experimental evidences, which showed that the inclined laminates that were not in contact with the masonry along all their length mobilise half the strain than the laminates in perfect contact with the masonry, averaging 75% overall. In Eq. (4) and Eq. (5), K represents the generic original property, and K* the modified one. These equations are valid for all the previously listed properties except the density: $E_{FRP}$, $f_{bFRP}$, $f_{sFRP}$ and $f_{tFRP}$. The modification of the density for the inclined cases does not need the ¾ factor. The variable $b_{FRP}$ is the width of the laminate (80mm) and $\bar{b}$ is the average width of the walls (833mm). It has to be noticed that assuming a linear distribution on the width of the wall of the FRP-masonry tensile and shear strengths is a first approach arisen from the bidimensional simplification that should be taking into account when analysing the results.

$$K^* = K \cdot \frac{\#_{v,FRP} \cdot b_{FRP}}{\bar{b}} \tag{4}$$

$$K^* = K \cdot \frac{3}{4} \cdot \frac{\#_{i,FRP} \cdot b_{FRP}}{\bar{b} \cdot sin \propto} \tag{5}$$

The calculated values of the mechanical equivalent properties are summarised in Table 6. In agreement with the experimental results, the horizontal laminates are not considered to directly contribute at the resistance of the walls against the bending/buckling phenomena so they have been not considered in the numerical model. It is also necessary to remark that the fracture energies corresponding to the tensile, shear or bonding strengths of the FRP have been calculated using Eq. (1) and these results are also presented in Table 6.

Finally, it was assumed that the contact between masonry and FRP was perfectly bonded (not sliding nor opening of the contact was allowed) at the positions (height) where laminates cross ones over others. This hypothesis is oriented to model the restraining effect that laminates might develop ones over others when they are applied following a crossed pattern (W#36-44 cases).

### *2.4.3. Mesh*

8-nodes uniform structured quadrilateral elements with quadratic integration of the displacements with an average size of 2mm was used to mesh the FRP.

**Table 6.** Modified properties of the FRP to model it as an equivalent uniform layer

| | $f^*_{tFRP}$ (MPa) | $f^*_{bFRP}$ (MPa) | $G^*_{f\,int}{}^{I}$ (N·m) | $f^*_{sFRP}$ (MPa) | $G^*_{f\,int}{}^{II}$ (N·m) | $\rho^*_{FRP}$ (kg/m$^3$) | $E^*_{FRP}$ (MPa) |
|---|---|---|---|---|---|---|---|
| Original FRP (^) | 3100 | 5.40 | 200 | 1.67 | 60.0 | 160.0 | 170000 |
| W#30-32 and W#36-38 | 595 | 1.04 | 38 | 0.32 | 11.7 | 30.7 | 32650 |
| W#33-35 and W#39-41 | 893 | 1.56 | 57 | 0.48 | 17.6 | 46.1 | 48980 |
| W#42-44 | 1021 | 1.78 | 65 | 0.55 | 20.2 | 70.3 | 56000 |

*(^)* The properties of the first row are not modified and correspond to the ones provided by the manufacturer or are directly calculated from these by using Eq. (1).

## 3. RESULTS AND DISCUSSION

The different versions of the numerical model described before have been applied to calculate the corresponding cases (unreinforced, TRM-strengthened or FRP-strengthened walls subjected to eccentric compressive load) in order to compare their results with the experimental ones.

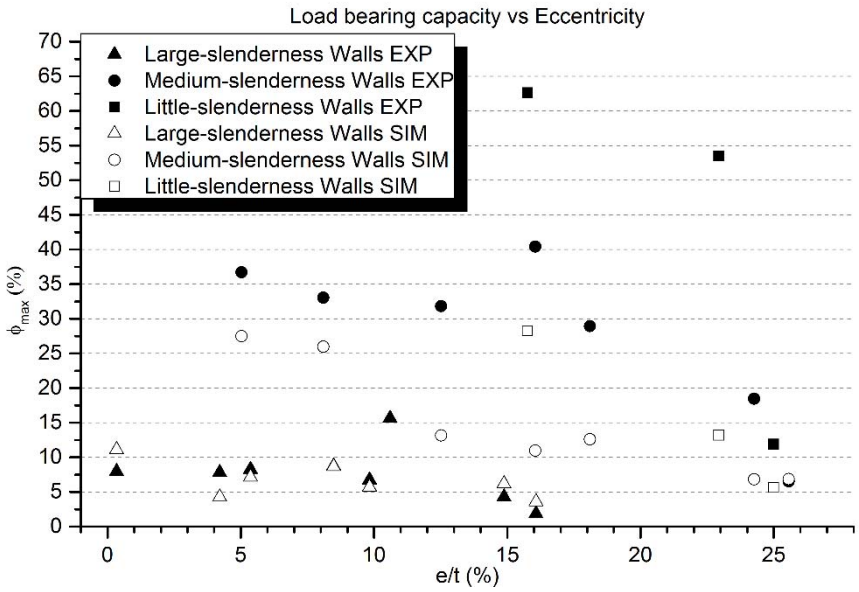


**Figure 4.** *Results for the Unreinforced brick masonry walls*

The model for unreinforced walls has been applied for all cases except Wall#5, whose experimental result was inconsistent with the rest of the experiments. Figure 4 shows the comparison between the experimental and simulated results. The graphs shows the dimensionless force ($\phi=F/F_u$ where $F_u$ is the maximum force that a cross section can bear under uniform compressed state) versus the dimensionless measurement of the eccentricity as the ratio of this parameter (e) out of the thickness of the wall (t). The best agreement is obtained for the most slender walls (W#1-W#9), with an average relative error of 38.4%. This accuracy level is acceptable because it is within the range of the common scatter obtained in the experimental tests. In fact, the scatter of the experimental results this study is compared with is larger than the average relative error of the numerical model. For the taller walls, the results show no general over- or underestimation. Thus, the proposed model behaves better for the

most slender walls. For the medium (W#10-16) and less slenderness (W#18-20) walls, the numerical results are consistently conservative. The error decreases as the eccentricity increases. This result indicates that the numerical model is more suitable for calculating the load-bearing capacity of slender and eccentrically loaded walls. The average relative errors are 43.2% and 61% for medium and little slenderness walls, respectively. However, the errors for the most eccentric tests are 5.1% and 52.8% for medium and less slenderness walls, respectively. The ultimate load calculated with the numerical model follows the trend of the experimental load measurement (see Figure 4) and is accurate within the limits of the experimental scatter. The behaviour of the model could be improved by implementing a constitutive equation to account for the over-strengthening of masonry in compression, e.g., the increase of the compressive strength for eccentric loading noticed by other authors [28]. The inclusion of the over-strengthening in compression would cause higher load-bearing capacities when the crushing failure process is significant, as in the case of less slender walls subjected to concentric or moderately eccentric loads.

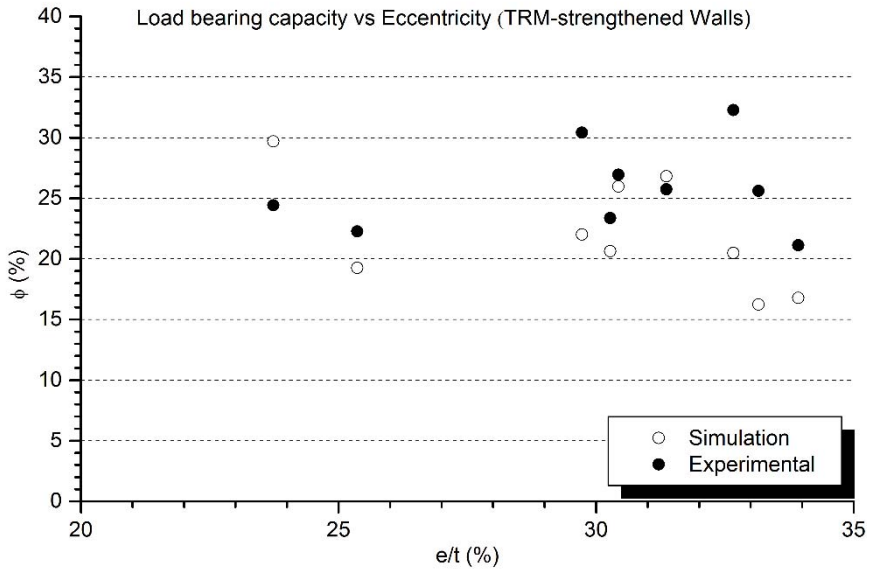


**Figure 5.** *Results for the TRM-strengthened brick masonry walls*

The results of the numerical simulations of TRM-strengthened walls and their comparison with the experimental evidences are represented in Figure 5. A relative error of 19.5% is obtained when comparing the numerically predicted load-bearing capacities with the experimental evidences. The model tends to underestimate the load-bearing capacity of the walls, especially in those cases whose eccentricity of the load is higher. In addition, the numerical results plotted in Figure 5 seem to point out that the eccentricity of the compressive load influences on the load-bearing capacity (the walls with major eccentricity are predicted to support minor loads). However, this tendency is not clear for the experimental results. Moreover, it has to be noticed that the proposed numerical model tends to underestimate the load-bearing capacity of the tested walls except for the cases strengthened with carbon fibre meshes. Also, it has to be said that proposed numerical model is applicable for a wide range

of cases (possible strengthening patterns) and affords the simulation of a large variety of failure modes. Finally, the dispersion of the numerically calculated load-bearing capacity of comparable walls is greater than the particular scattering of the experimental tests in this case (comparing walls W#21 and W#22 between them and W#23 with W#24).

Figures 6, left shows the tangential stress distribution along the fictitious inclined contacts of the masonry for a case which fails due to masonry compressive/shear collapse near the ends of the wall, according with the numerical results. In this figure, the circled parts of the contact lines have reached the shear strength. This situation affects more than a half of the contact line causing the failure of the wall.

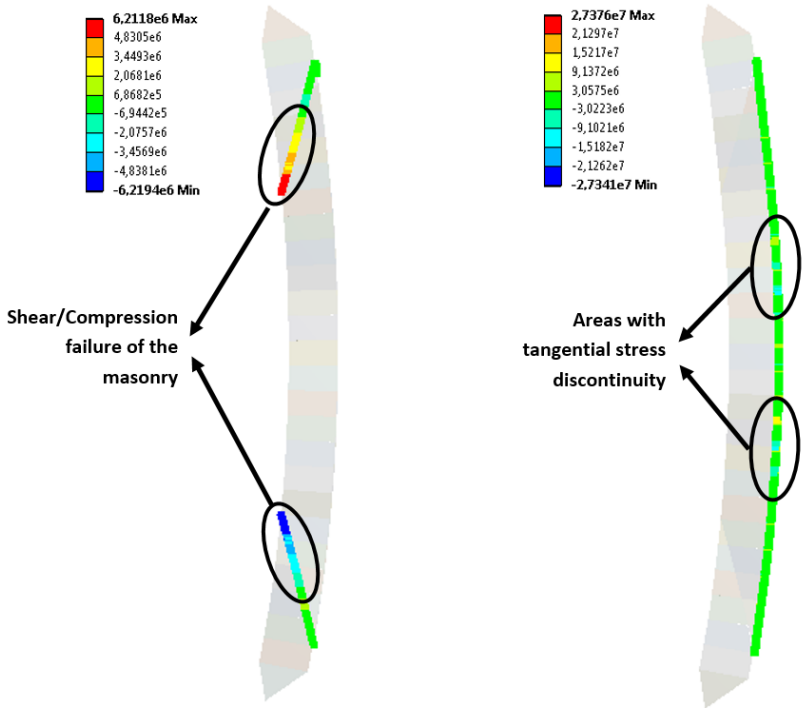


**Figure 6.** *Numerical simulation of the inclined contacts of the masonry (left) and the contacts between the masonry and the FRP (right)*

The results of the numerical simulations of the FRP-strengthened walls are presented in Table 7. The third, fourth and fifth columns of this table correspond to the dimensionless values of the vertical displacement, lateral displacement at mid-height and applied force at the failure moment. The predicted load bearing capacity of each wall is shown in the sixth column, whereas the seventh column summarises the absolute value of the relative error of the calculated ultimate load in comparison with the experimental value. In the last column, the average error for each series is shown. Observing the results of this table, it has to be highlighted that the implemented finite element analysis tends to overestimate the load-bearing capacity of the studied walls. The load-bearing capacity is predicted with an average error of 25.1%, which is within the typical scattering of experiments on masonry structures (around 30%). Taking all this information together, it seems likely that the used definition of the applied FRP might be stiffer than the real solution in the vertical direction but more flexible than the used material in the lateral orientation. This effect might be explained by the contribution of the adhesive layers, which were not considered in the model and were thicker than proposed by the producers due

to applicability limitations, combined with the possible underestimation of the Young's modulus of the masonry. In this line, placing a thicker layer of adhesive might have contributed to limit the experimental lateral deformation of the tested walls because it means introducing an additional material stiffer than masonry. Furthermore, the error of the numerical model might be related with the definition of the materials. In particular, the compressive behaviour of the masonry and the fracture energies of masonry, FRP and interfaces between them might be defined in a more realistic way to model the experimental response of the studied structures with more accuracy. Regarding the compressive response of the masonry, two improvements are possible: implementing a parabolic stress-strain compressive response and using a more representative value of the Young's module. However, the first improvement will be against the aim of keeping the model definition as simple as possible. The possible underestimation of the Young's modulus of the masonry used in the numerical model might explain the error in the lateral deformation. In addition, higher values of the Young's modulus of the masonry would result in lower lateral deformations and a better adjustment of the experimental data. In contrast, increasing the Young's modulus of the masonry will derive in a larger load-bearing capacity, accentuating the current overestimation trend of the model, so other variables seem to be necessarily changed. About the fracture energies, it seems necessary to develop analytical approaches to determine each fracture energy as function of the corresponding strength among other possible parameters. This improvement will provide a scientifically justified alternative to the first approach of using of the same relationship for all fracture phenomena, which has been adopted herein to avoid providing arbitrary values. In fact, the used definition of the fracture energies might explain a great deal of the obtained error and improving it would help to reach more accurate results. Another simplification which might have contributed to the error of the numerical model is the uniform linear distribution of the mechanical properties of the discrete strengthening system (laminates) along the width of the wall to allow the bidimensional hypothesis. This fact might be related with the overestimation of the load-bearing capacity of the walls because the used simplification assumes a uniform stress distribution on the interfaces although it is known that, for example, the tangential stress distribution is not uniform and there are sections with minor shear strength than the assumed one.

In addition, for the FRP-strengthened cases, the predicted failure modes shows agreement with the experimental observations. In particular, reaching the tangential strength of the fictitious inclined contact in the masonry near the ends of the wall is pointed out as the collapse cause of the studied FRP-strengthened walls in agreement with the numerical results. In addition, it has to be remarked that the definition of the contacts oriented to represent the effect of the laminates crossing over others causes a particular stress distribution in the masonry-FRP contact (see Figure 6, right). In fact, there is a slight discontinuity in the tangential stress distribution due to the bonded restrain imposed at the positions where the laminates were crossed (1/3 and 2/3 of the wall's height for the W#38 case represented in Figure 6 right). This result indicates that the restraining effect of the horizontal laminates might lead to increasing the tangential stress of the masonry-FRP contact in punctual areas, which might cause adherence problems in the simulated model. Thus, installing horizontal crossing laminates to avoid the debonding phenomena might be counter-productive because the tangential stress distribution of the vertical ones is modified increasing the possibility of a punctual sliding failure that starts a global failure of the laminate adherence. However, this ultimate effect has not been experimentally observed nor numerically predicted.

**Table 7.** Results of the numerical model at calculating FRP-strengthened walls

| Wall | $v_{max}/H_{ef}$ ($\cdot 10^{-3}$) | $h_{max}/t$ (%) | $\phi_{max}$ (%) | $F_{max}^{SIM}$(kN) | Abs. rel. err. (%) | Av. err. (%) |
|---|---|---|---|---|---|---|
| W#30 | 5.2 | 30.0 | 33.6 | 763.4 | 45.8 | |
| W#31 | 5.0 | 29.7 | 31.1 | 707.0 | 28.9 | 26.9 |
| W#32 | 3.1 | 16.0 | 25.9 | 587.6 | 6.0 | |
| W#33 | 4.8 | 26.1 | 34.0 | 761.8 | 27.3 | |
| W#34 | 4.6 | 24.7 | 33.1 | 745.7 | 24.1 | 18.8 |
| W#35 | 4.3 | 23.2 | 31.5 | 713.4 | 5.0 | |
| W#36 | 3.3 | 17.2 | 26.8 | 610.3 | 1.0 | |
| W#37 | 3.6 | 20.3 | 24.5 | 545.0 | 9.3 | 8.1 |
| W#38 | 4.8 | 28.4 | 31.9 | 703.9 | 13.9 | |
| W#39 | 4.6 | 24.9 | 32.7 | 722.1 | 32.4 | |
| W#40 | 3.6 | 18.5 | 30.7 | 681.7 | 30.0 | 36.5 |
| W#41 | 3.7 | 19.4 | 30.0 | 665.6 | 46.9 | |
| W#42 | 4.2 | 22.1 | 33.8 | 744.0 | 15.6 | |
| W#43 | 4.3 | 22.8 | 32.6 | 722.0 | 59.8 | 35.4 |
| W#44 | 4.4 | 23.2 | 34.0 | 746.0 | 31.0 | |

Comparing the results of the finite element analysis among them, it is noticed that restraining the masonry-FRP contacts to represent the presence of horizontal laminates causes a load-bearing capacity decrease (comparing W#30-32 with W#36-38 and W#33-35 with W#39-41). This is in line with the previous comment. Thus, according with the model, and for the proposed structural configuration and loading pattern, including horizontal FRP laminates is not effective. In contrast, the model reproduces the effect of installing three vertical laminates (W#33-35) in comparison with the cases with two laminates (W#30-32). A minor load-bearing capacity increase is predicted when adding vertical laminates as experimentally observed. Finally, it has to be remarked that the average load bearing capacity predicted by the model for the cases W#42-44 and W#33-35 are practically the same. This fact supports the hypothesis of assuming a reduction factor (¾) for the FRP properties associated with inclined laminates in the described configuration.

## 4. CONCLUSIONS

The objective of implementing a numerical model, which was capable of predicting the load-bearing capacity of Unreinforced, TRM-strengthened and FRP-strengthened walls subjected to eccentric compressive load at a low computational cost, has been achieved. The particular adaptation for each case have bring specific conclusions. Thus, for the simulation of unreinforced walls, it might be concluded that the numerical model is more accurate for the cases with high eccentricity and more slenderness. In addition, the obtained results emphasise that a realistic description of the joint behaviour is essential to accurately predict the load-bearing capacity of unreinforced masonry walls, especially when the failure mode is primarily second-order bending.

Regarding TRM-strengthened walls, it is important to remark that the load-bearing capacity predicted by the model correctly adjusts the experimental results. The average error is within the typical experimental scattering of destructive tests on masonry walls, around 30%, and it is better than the error obtained for the unreinforced walls. This fact agrees with the greater uniformity of the structural

response showed by the TRM-strengthened walls in comparison with the behaviour of unreinforced masonry walls. In addition, it can be concluded that the influence of the compressive strength of the masonry and its Young's modulus is very significant in those cases with small load eccentricities, which failed by shear/compression. In contrast, the response of the walls that fail due to bending/buckling phenomena, which are the ones with the larger load eccentricities and/or slenderness, is less influenced by these parameters. Moreover, the load-bearing capacity of the walls subjected to larger load eccentricity tends to be underestimated by the proposed numerical model. A conservative definition of the mechanical variables which directly describe the bending response of the walls might explain this underestimation tendency.

Also in relation with the numerical modelling of TRM-strengthened walls, it is worth noticing that the numerical model only overestimates the experimental cases of the walls strengthened with carbon fibre grids. This result might point out that the adherence between the inorganic matrixes and the carbon fibre grids is not reliable. Finally, it has been observed that the compressive/shear failure mode happens, in the numerical simulations, when the shear strength is reached in more than a half of the considered dividing line on the masonry.

The analysis of the results of the numerical simulation of FRP-strengthened walls, allows concluding that the proposed model accurately predicts the experimentally observed failure mode and the small influence of the strengthening pattern on the resistance of the analysed cases. In addition, it might be concluded that a significant part of the error of the numerical model might be due to the approximate and maybe controversial definition of the fracture energies.

As general conclusions, it is important to highlight that considering a more realistic formulation to represent the compressive response of the masonry might help improving the obtained results. In addition, a realistic Young's modulus must be used because it determines the deformation leading to the geometric instability associated with buckling failure. Thus, future works might include accurately obtain the Young's modulus of masonry elements, performing parametric analyse or developing three-dimensional models including the out-of-plane shear in the study.

## ACKNOWLEDGEMENTS

The authors would like to acknowledge the support of the companies BASF, MAPEI and RUREDIL who provided the strengthening materials for carrying out the experimental part of the current research. In addition, we would like to recognise the collaboration of COMSA-EMTE at the development of the research about FRP strengthening techniques.

## REFERENCES

[1] Corradi, M., Borri, A., Vignoli, A. (2002). Strengthening techniques tested on masonry structures struck by the Umbria–Marche earthquake of 1997–1998. *Construction and Building Materials, 16, 229–239.*

[2] Bernat, E., Gil, L., Roca, P., Escrig, C. (2013). Experimental and analytical study of TRM strengthened brickwork walls under eccentric compressive loading. *Construction and Building Materials, 44, 35–47.*

[3] Baratta, A., Corbi, O. (2007) Stress analysis of masonry vaults and static efficacy of FRP repairs. *International Journal of Solids and Structures, 44, 8028–8056.*

[4] Papanicolaou, C.G., Triantafillou, T.C., Karlos, K., Papathanasiou, M. (2006). Textile-reinforced mortar (TRM) versus FRP as strengthening material of URM walls: in-plane cyclic loading. *Materials and Structures, 40, 1081–1097.*

[5] Papanicolaou, C.G., Triantafillou, T.C., Papathanasiou, M., Karlos, K. (2007). Textile reinforced mortar (TRM) versus FRP as strengthening material of URM walls: out-of-plane cyclic loading, *Materials and Structures, 41, 143–157.*

[6] Augenti, N., Parisi, F., Prota, A., Manfredi, G. (2011). In-Plane Lateral Response of a Full-Scale Masonry Subassemblage with and without an Inorganic Matrix-Grid Strengthening System. *Journal of COmposites for Construction, 15, 578-590.*

[7] Papanicolaou, C., Triantafillou, T., Lekka, M. (2011). Externally bonded grids as strengthening and seismic retrofitting materials of masonry panels. *Construction and Building Materials, 25, 504–514.*

[8] Harajli, J., ELKhatib, M.H., Tomas San-Jose, J. Masonry Walls Strengthened Using Fibre Textile-Mortar System: Experimental Evaluation of Out-of-Plane Cyclic Response. In: CSHM-3 (pp. 19–32). Ottawa-Gatineau, Canada.

[9] García, D. (2009). Experimental and numerical analysis of stone masonry walls strengthened with advanced composite Materials (PhD. Thesis). Bilbao: Escuela de Ingenieria de Bilbao.

[10] Dawe, J.L., Liu, Y. (2003). Analytical modeling of masonry load-bearing walls. *Canadian Journal of Civil Engineering, 30, 795-806.*

[11] Martini, K. Finite element studies in the two-way out-of-plane failure of unreinforced masonry. In 6th National COnference on Earthquake Engineering (pp.1-12). Seattle: Earthquake Engineering Research Institute.

[12] Lourenço, P.B. (1994). Analysis of masonry structures with interface elements. Theory and applications. Delft: TNO Building and Construction Research.

[13] Sacco, E. (2009). A nonlinear homogenization procedure for periodic masonry. *European Journal of Mechanics Part A/Solids, 28, 109-222.*

[14] Milani, G., Lourenço, P.B., Tralli, A. Homogenised limit analysis of masonry walls, Part I: Failure surfaces. *Computers and Structures, 84, 166-180.*

[15] Bernat-Maso, E., Gil, L. Numerical study of the performance of TRM strengthened brickwork walls against second order bending effects. In 9th International Masonry Conference (pp. 1-12). Guimaraes: Universidade do Minho. Departamento de Engenharia Civil.

[16] Larrinaga, P., Chastre, C., Biscaia, H.C., San-José, J.T. (2014). Experimental and numerical modeling of basalt textile reinforced mortar behavior under uniaxial tensile stress. *Materials and Design, 55, 66-74.*

[17] Carozzi, F.G., Milani, G., Poggi, C: (2014). Mechanical properties and numerical modeling of Fabric Reinforced Cementitious Matrix (FRCM) systems for strengthening of masonry structures. *Composite Structures, 107, 711-725.*

[18] Elsanadedy, H.M., Almusallam, T.H., Alsayed, S.H., Al-Salloum, Y.A. (2013). Flexural strengthening of RC beams using textile reinforced mortar – Experimental and numerical study. *Composite Structures, 97, 40-55.*

[19] Al-Salloum, Y.A., Elsanadedy, H.M., Alsayed, S.H., Iqbal, R.A. (2012). Experimental and Numerical Study for the Shear Strengthening of Reinforced Concrete Beams Using Textile-Reinforced Mortar. *Journal of Composite Construction, 16, 74-90.*

[20] Cecchi, A., Milani, G., Tralli, A. (2004). In-plane loaded CFRP reinforced masonry walls: mechanical characteristics by homogenisation procedures. *Composite Science Technology, 64, 2097-2112.*

[21] Milani, G. (2008). Homogenized limit analysis of FRP-reinforced masonry walls out-of-plane loaded. *Computational Mechanics, 43, 617-639.*

[22] Bernat, E., Gil, L., Roca, P., Sandoval, C. (2013). Experimental and numerical analysis of bending–buckling mixed failure of brickwork walls. *Construction and Building Materials, 43, 1–13.*

[23] Bosiljkov, V., Totoev, I.Z., Nichols, J.M. (2003). Shear modulus and stiffness of brickwork masonry : An experimental perspective. *Structural Engineering and Mechanics, 20, 21-44.*

[24] Alfano, G., Crisfield, M.A. (2001). Finite Element Interface Models for the Delamination Anaylsis of Laminated Composites: Mechanical and Computational Issues. *International Journal of Numerical Methods in Engineering, 50, 1701-1736.*

[25] Pluijm, R. Material properties of masonry and its components under tension and shear. In 6th Canadian Masonry Symposium (pp. 675-686). Saskatoon, Saskatchewan, Canada: V.V. Neis.

[26] Sandoval, C., Roca, P., Bernat, E., Gil, L. (2011). Testing and numerical modelling of buckling failure of masonry walls. *Construction and Building Materials, 25, 4394-4402*.

[27] Bernat-Masó, E., Sandoval, C., Gil, L., Roca, P. Numerical modeling for the prediction of the buckling failure of masonry walls. In XXXVII IAHS World Congress on Housing Science. Santander: L. Villegas

[28] Brencich, A., Corradi, C., Gambarotta, L. (2008). Eccentrically loaded brickwork: Theoretical and experimental results. *Engineering Structures, 30, 3629-3643.*